Scripta Materialia 113 (2016) 122–126

Contents lists available at ScienceDirect

Scripta Materialia

journal homepage: www.elsevier.com/locate/smm

Precise strain profile measurement as a function of depth in thermal barrier coatings using high energy synchrotron X-rays

C. Li [a], S.M.D. Jacques [a], Y. Chen [a], P. Xiao [a], A. Beale [c], M. di Michael [b], N. Markossan [d], P. Nylen [d], R.J. Cernik [a,*]

[a] School of Materials, University of Manchester, M13 9PL, UK
[b] ESRF-The European Synchrotron, 71, Avenue des Martyrs, Grenoble, France
[c] University College London, RCaH Rutherford Appleton Laboratory, Harwell Oxford Didcot Oxon, OX11 0FA, UK
[d] Production Technology Centre, University West, Trollhättan, Sweden

ARTICLE INFO

Article history:
Received 19 August 2015
Received in revised form 9 October 2015
Accepted 17 October 2015
Available online xxxx

Keywords:
Thermal barrier coatings
High energy synchrotron powder diffraction

ABSTRACT

We have developed a method of directly measuring the strain gradient as a function of depth in plasma sprayed Thermal Barrier Coatings (TBCs). A 92.8 keV monochromatic synchrotron X-ray beam was used to penetrate the 10 × 10 × 8 mm samples in transmission geometry. The samples had been heated to 1150 °C and held at that temperature for 190 h. The diffraction patterns were collected using a DECTRIS pilatus3 X CdTe 300 K area detector. The patterns were analyzed by partial circular integration followed by full Rietveld refinement to obtain the lattice parameters of the TBC top coat at 25 μm intervals as function of depth. The coatings surviving the heat treatment process without significant damage were found to exhibit a variable compressive stress state inside the top coat. This was found to be about −600 MPa at the bond coat interface decreasing in a non-linear fashion towards the surface. By refinement of the data collected from sectors of whole Debye Scherrer rings we were able to estimate both the in-plane and out-of-plane strain.

© 2015 Elsevier B.V. This is an open access article under the CC BY license (http://creativecommons.org/licenses/by/4.0/).

Introduction

Residual stress is a serious problem that is implicated in the failure mechanisms of ceramic/metal layered structures such as TBCs [1–2] and brazed joints [3–4]. TBCs are widely used as coating materials for super alloys used in jet engine turbine blades. The application of the TBC allows higher working temperatures and improved efficiency [5–7]. However, as Zhao and Xiao et al. discuss, TBC failure mechanisms are not currently well understood and suggest, for this reason, that the material application has not yet reached its full potential [8]. The driving force for most failures of APS (Atmosphere Plasma Spray) TBCs is the residual stress generated by thermal mismatch between the top coat and substrate. Thus it is necessary to investigate the residual stress distribution accurately as a function of depth in the TBC top coat.

A large number of methods have been applied to measure the residual stress distributed in TBC systems. Raman Spectroscopy [9–12] is commonly used to measure residual stress in the TBC top coat. However, since zirconia is transparent to most Raman lasers, the beam will spread in top coat, resulting in a large interaction volume making it difficult to localize the scattering source within the coating. In addition, Limarga et al. [11–12] pointed out that the PS (Piezo-Spectroscopic) coefficient representing relationship between the peak shift and stress can be affected by the microstructure and heat treatment, which needs to be calibrated and is also difficult to determine. New developments in near field photoluminescence [13] can achieve high spatial resolution in TGO stress measurement and the resolution of measurement can be greatly improved. However, the relatively shallow penetration depth of the laser into the material makes it difficult to achieve the average value of the stress distributed in top coat.

Standard laboratory based XRD [14] is another commonly used method for residual stress measurement. However, the penetration depth of these X-rays (typically 8–17 keV) is very limited due to the high density and high absorption of the top coat. Therefore measuring the strain distribution across the thickness of an as-manufactured coating (~250 μm) is not possible. Synchrotron sources offer very high energy monochromatic X-rays with very high flux coupled with high brightness. This makes it possible to measure the residual stress distribution in thick materials such as our zirconia TBCs accurately and efficiently [15–17]. A recent paper [18] reported experiments on the strain response of TBCs under high temperatures and loading conditions. However, due to the cylindrical geometry of their sample, the strain distribution (as a function of depth) was provided as a trend towards the surface but always contained scattering from deeper levels. This information content is similar to that obtained by the measurement technique employed by Scurr et al. [19]. when examining natural ceramics. Some researchers [20–21] have used transmission geometry to investigate on the strain distribution in TBCs but the sample was

* Corresponding author.

http://dx.doi.org/10.1016/j.scriptamat.2015.10.032
1359-6462/© 2015 Elsevier B.V. This is an open access article under the CC BY license (http://creativecommons.org/licenses/by/4.0/).

cut after heat treatment, which is known to cause relaxation and redistribution of residual stress. Also, the sample thickness is only 2.5 mm, the geometry of which is too small to represent the real operational case.

To overcome these difficulties we have developed a method to precisely measure the strain distribution in a TBC top coat as a function of depth in 25 μm steps. We used high energy monochromatic synchrotron radiation using a small beam cross-section coupled with an area detector. The whole Debye–Scherrer ring pattern can be measured which gives the capability to separate out the in-plane and out-of-plane strain components. A novel way to analyze the data to reveal strain distributions in the TBC by Rietveld refinement is described and the changing trend of lattice parameter (and hence strain) as a function of depth is reported.

The thermal barrier coatings in this study were fabricated by Atmosphere Plasma Spray (APS) at University West. The top coat is made of 8 wt.% Yittra Stabilized Zirconia (YSZ) with thickness of 250 μm and the content of the bond coat is NiCoCrAlY fabricated by APS. The thickness of the bond coat is 150 μm on a Hastelloy substrate. The samples were cut into 10 mm × 10 mm × 8 mm pieces before heat treatment to ensure the sample was large enough to represent the biaxial residual stress state in a realistic operating environment. Heat treatment was carried out in Cabolite muffle furnace at 1150 °C for 190 h. The diffraction experiment was carried out at beamline ID15A, ESRF, France. A DECTRIS Pilatus3 X CdTe 300 K area detector was used to collect the diffracted signal. The detector has 487 × 619 172 μm^2 pixels arranged in six blocks (3 × 2).

The experiment was carried out in transmission geometry as shown in Fig. 1a. The high energy beam penetrated the entire length (~10 mm) of the sample and the diffraction pattern was recorded by the CZT DECTRIS area detector. Fig. 1(a) shows an absorption contrast image taken with a large beam cross section. The nickel super alloy appears lighter than the TBC and a thin, thermally grown, oxide layer (TGO) is faintly visible. The detector was mounted orthogonal to the beam path and centered on the beam to collect a large sample of the Debye–Scherrer rings (sample to detector distance dependent). The sample could then easily be translated horizontally across the beam (Fig. 1b) thereby sampling the TBC at different depths. Fig. 1b position 1 shows the beam and resultant image when penetrating the Hastelloy substrate, the single crystal nature is shown by the spotty pattern and one exit beam from a large single crystal has acted as a secondary incident beam giving a small zirconia powder pattern. Fig. 1b position 2 shows the mid TBC position when a highly textured EBPVD sample was irradiated. Finally Fig. 1b position 3 shows powder pattern obtained from the APS TBC studied in this paper. The depth from the surface in this case was approximately 50 μm. The pattern is brighter on the right hand side because the absorption pathways for the exit beam were shorter. This intensity balance was observed to balance out as expected towards the center of the TBC.

The method also measures diffraction from crystallites located at different angles within the sample so lattice parameters refined from orthogonal integrated sectors can be used to determine the strain in and out-of-plane.

The energy of the beam was 92.8 keV and the beam size was 25 μm × 40 μm. Initially the beam was positioned at the grazing incidence position on the sample surface indicated by the appearance of zirconia rings instead of air scattering. The sample was moved in 25 μm steps causing the interaction volume to move towards the interface. The interface position was determined to be at the position where alumina peaks from the thermally grown oxide began to emerge. The working distance of the detector was 500 mm, which was calibrated by FIT2D (Hammersley, 1995) using a CeO_2 NIST standard. The diffraction rings were analyzed by FIT2D. The rings were partially integrated in-plane over a 16° sectors to obtain the one dimensional powder diffraction pattern. As shown in Fig. 1 b position 3). The integrated pattern was refined by the TOPAS program (Bruker-AXS, Germany). The zero error and LP factors were fixed to zero. The background was modeled

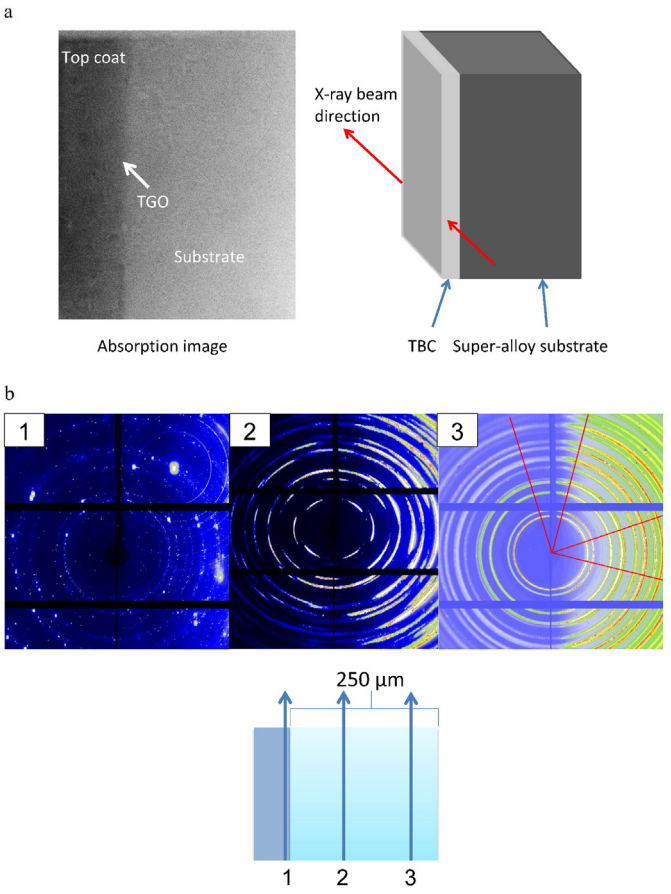

Fig. 1. a. Experiment geometry showing the presentation of the sample to the beam and absorption image in transmission showing the substrate, TGO and TBC b. Three images at different depths in the specimen. Position 1 shows the diffraction pattern collected from the beam penetrating the substrate. The diffraction rings are very spotty demonstrating diffraction from a few large crystallites. One particularly large reflection is responsible for acting as a secondary incident beam giving a zirconia pattern from the top coat. Position 2 shows the diffraction pattern from an EBPVD sample (not part of this study) showing strong preferred orientation; this is another parameter that can be measured as a function of depth. Position 3 shows the diffraction from an APS sample closer to the surface than the interface. The intensity mismatch arises because of the relative absorption pathways.

by Chebychev polynomials of 2th order. The peaks shape was a good fit to the Thomlinson et al. modified pseudo Voigt function [22]. Given the highly symmetric nature of the materials the only refinable structural parameters were the lattice parameter and average crystallite size. The tetragonal phase was refined, as a start point, using the Bondars [23] structure model based on a tetragonal cell ($P4_2/nmc$). After measurement, the sample was cross-sectioned by a slow speed cutting wheel then ground and polished to a 60 nm rms roughness. The microstructure was observed by scanning electron microscopy (SEM, Quanta 650, FEI) operated in low vacuum mode.

The typical microstructure of the APS samples after heat treatment is shown in Fig. 2. It can be seen that, the top coat is relatively uniform with some small inter-splat cracks but with no cracks large enough to cause failure.

A thermally grown oxide (TGO) can be observed at the interface between top coat and bond coat. The TGO contains two layers: a gray spinel layer on the top and a dark alumina layer below [8].

The penetration depth of the beam can be calculated by $\frac{I}{I_0} = e^{-\mu\tau}$, where I and I_0 are the intensity of the beam after and before penetrating the material, μ is the linear absorption coefficient and τ is the penetration depth of the beam. The intensity arriving at the area detector is

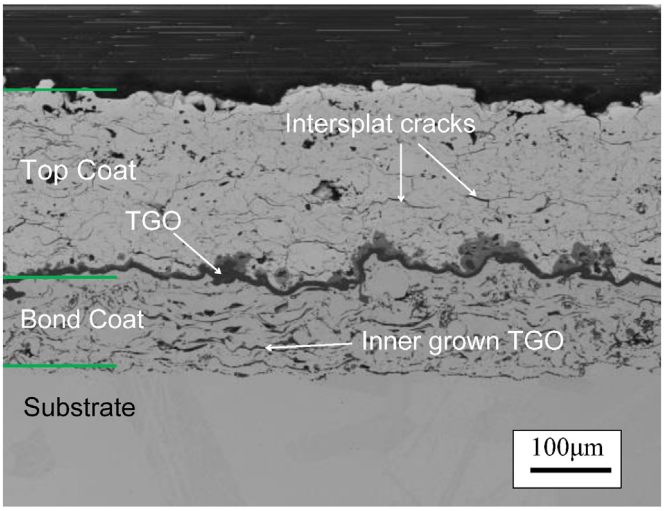

Fig. 2. SEM of an APS TBC heat treated at 1150 °C for 190 h showing the irregular grain structure originating from the APS manufacturing process.

the integral of the intensity of the diffracted beam from a certain distance in the sample. So the average intensity shown on the area detector can be calculated from $I_0\int_{\tau_1}^{\tau_2} e^{-\mu\tau}d\tau = -I_0\frac{1}{\mu}(e^{-\mu\tau_2}-e^{-\mu\tau_1})$, where τ_1 and τ_2 are the limits of the beam penetration. When the weakest part of Debye–Scherrer the ring is about 80% of the strongest part the penetration depth corresponds to about half of the total sample thickness (~4 mm). Since the stress state in the sample can be regarded to be symmetric, the data collected in our experiment should be able to represent the real residual stress state in top coat. Fig. 1 b) position 3 shows an example of the Debye- Sherrer ring of the top coat. The intensity of the rings is relatively uniform over their entire circumference, although some bright spots can be observed. The footprint of the beam is very small so it can encounter some large crystallites which are comparable to the size of the beam. If this crystallite happens to be in the diffraction position it can generate very strong diffraction and result in a spotty pattern. But most of the patterns transferred from the caked part show a relatively symmetric peak shape and few grainy features so this effect was negligible. For the Rietveld refinement the background, lattice parameter and average crystallite size were refined. This relatively simple model was found to give very reproducible results with an average goodness of fitting (GOF) of around 1.1, where GOF = $chi^2 = \frac{R_{wp}}{R_{exp}} = \sqrt{\frac{\sum w_m(Y_{o,m}-Y_{c,m})^2}{M-P}}$, $Y_{o,m}$ and $Y_{c,m}$ are the observed and calculated data, w_m is the weighting given to data point m, M is the number of the point and P is the number of parameters [24]. Fig. 3 shows three examples of refinement results of the pattern. The first pattern in Fig. 3 was recorded with the beam parallel and very close to the sample surface. The peak intensity of this pattern is relatively low and the background is higher than the other cases. The relatively low intensity of the pattern and high background can be attributed to two reasons. Firstly, when the beam is glancing incident on the ceramic/air interface, there can be some reflection of the beam at the interface, which can contribute to the relatively high background. Secondly, at this time, only part of the beam is inside the sample, resulting in less volume of the material is scattering the beam. Thus the intensity of the diffracted beam is relatively lower than the others. The second pattern was measured when the whole beam is in the sample and peak intensity is much stronger than the first one. The third pattern shown was measured when the beam reached the interface and the peak of alumina (TGO). According to the refinement, about 71% of the beam is in the top coat while the other part is in TGO. It can be seen that our model is a good fit to the detected diffraction pattern and the gray line representing the difference between the original pattern and the refined pattern is small as is the error in refined lattice parameter (0.015 Å). When the beam is exiting the sample, the direction of the beam may be changed due to the difference in the index of refraction. And then index of refraction of X-Ray can be calculated [25] by $n = 1 - \delta$ and $\delta = 1.3 \times 10^{-6}\rho\lambda^2$, where n is the

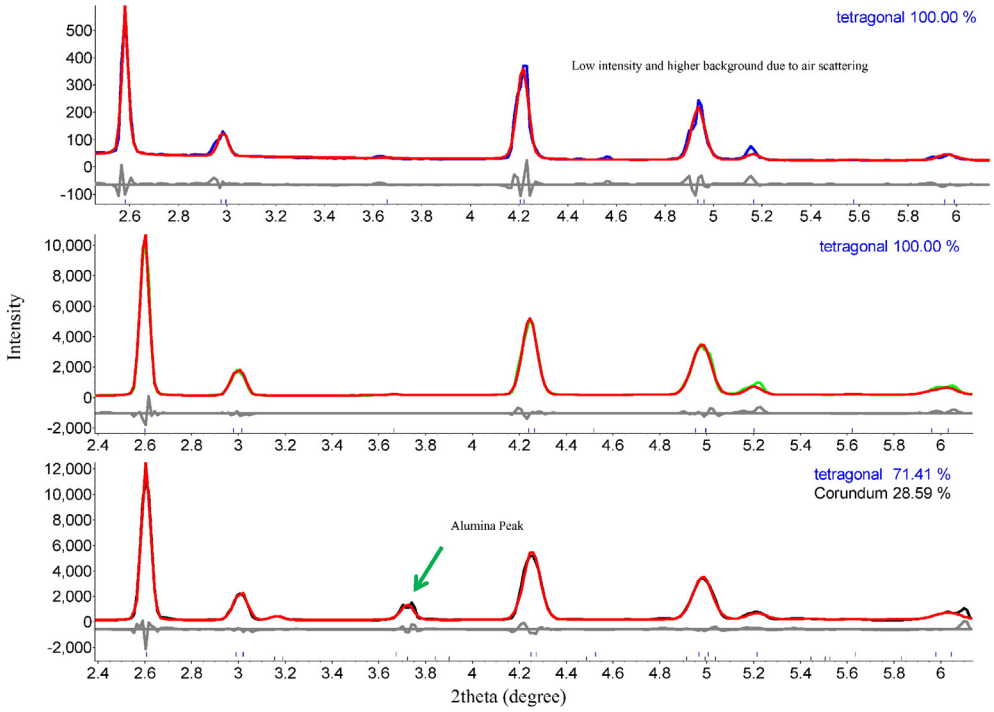

Fig. 3. The refined diffraction patterns from 3 depths, the interface is shown by the presence of alumina from the TGO. The observed pattern is shown in blue, calculated red and difference in gray. The ticks show the positions of the expected Bragg peaks. (For interpretation of the references to color in this figure legend, the reader is referred to the web version of this article.)

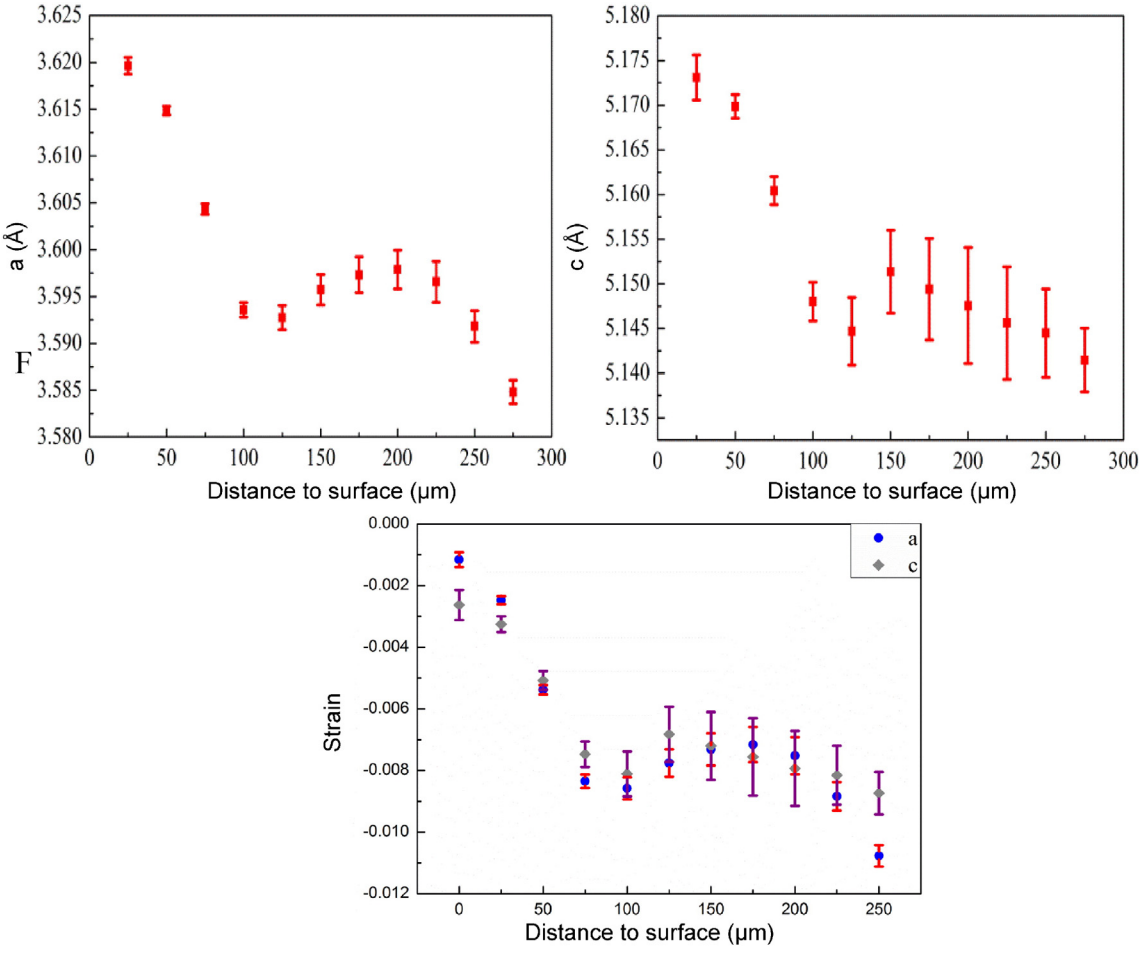

Fig. 4. The in-plane trend in lattice parameters as a function of depth. This compressive, non-uniform trend was observed in all the undamaged, heat treated samples. The corresponding change in strain is also shown normalized to the surface state.

index of refraction of X-Ray in zirconia, δ is the difference between 1 and the X-ray index of refraction in zirconia, ρ is the density and λ is the wavelength of X-ray which is 0.133621 Å in our experiment. The theoretic density of zirconia is 6.2 g/cm^3. After calculation, the difference between index of X-ray in air and in zirconia $\delta = 1.43908 \times 10^{-7}$. From which it can be seen that the difference is very small, so the effect of refraction can be neglected.

Fig. 4 shows the change of the in-plane lattice parameter and the strain calculated according to the lattice parameters achieved as a function of distance to surface. Both lattice parameters show similar trend. It can be seen that the lattice parameter is generally decreasing when approaching the TGO/top coat interface. In the first 100 μm from the surface, the lattice parameter decreases rapidly, and then the lattice parameter increased a little in the next 50 μm dropping again with a smaller gradient than the first part. This non uniform behavior was observed in all samples that survived the heat treatment without developing large cracks. As indicated by Limarga et al. [11], the peak position shift can also be caused by possible phase transformation. To prove the peak shift reported here is only caused by residual stress inside the coating. The top coat was soaked off the substrate by HCl, and a series of tests including Energy-Dispersive X-ray Spectroscopy (EDS) measurement, Raman Spectra and laboratory based XRD were carried out. The results show that the change of lattice parameters are caused by the residual stress and not by other possible reasons (i.e. inhomogeneous element distribution, or possible phase transformation). The residual stress in TBCs mainly generate from the thermal mismatch between top coat and substrate so a compressive stress state in top coat is expected. The decreasing trend of the lattice parameters indicates an increase of compressive stress state inside the top coat. The constraint of the top coat comes from the substrate below and the surface is expected to be free to relax, so the stress is also expected to increase from surface to the interface, resulting in a decreasing value of lattice parameter. The strain was then calculated by $\varepsilon = \frac{a-a_0}{a_0}$ or $\varepsilon = \frac{c-c_0}{c_0}$, where ε is the strain, a_0 and c_0 are the stress free lattice parameters and a and c are the lattice parameters of the material under compressive stress. The value of a_0 and c_0 needs to be calculated. For the sample surface, the out-of-plane stress is zero and thus the out of plane strain is only due to the Poisson effect. According to Poisson effect, it can be inferred that $2\epsilon_1 \upsilon = \epsilon_2$, where ϵ_1 is the in-plane strain, υ is the Poisson ration which is taken as -0.3 and ϵ_2 is the out-of-plane strain. The stress free lattice parameters a_0 and c_0 can be calculated from $2\frac{a_1-a_0}{a_0}\upsilon = \frac{a_2-a_0}{a_0}$ and $2\frac{c_1-c_0}{c_0}\upsilon = \frac{c_2-c_0}{c_0}$, where a_1 and c_1 are the lattice parameters refined from in-plane direction and a_2 and c_2 are the lattice parameters refined from out-of-plane direction. The calculated value of a_0 and c_0 are $a_0 = 3.625$ and $c_0 = 5.1825$. It can be seen that the strain calculated by a and c exhibits a similar trend. The increasing trend of compressive stress from surface to the interface also agrees well with the values measured in the references [26–28]. The small difference between the value calculated by a and c may be attributed to the different deformation ability of different direction of zirconia crystals. But we are still not clear why there is an increase in the middle of the curve. The compressive stress state and the increase of the stress from surface to the interface are also reported by many researchers using curvature method [26–27] and Raman spectra

[9–10,29]. If the young's modulus of top coat is taken as 60 GPa, which is usually the value being reported, the stress value at the interface is estimated to be around 600 MPa. This value is similar to that reported by Xiaofeng et al. [29] who used indentation method and (photoluminescence piezo-spectroscopy) PLPS method to measure the residual stress in (Electron Beam Physical Vapor Deposition) EBPVD top coat and reported a compressive stress around 500 MPa in top coat after heat treatment. These authors also observed a similar trend which increased rapidly at first, then started to slow down. J. Thornton et al. [20–21] also observed a similar trend on the strain of the APS top coat though they used a thinner sample. This was attributed to the highly heterogeneous structure of the APS films. Our result shows a trend different from most theoretic models and (Finite Element Method) FEM models. The authors believe that this is attributed to the complex microstructure of TBC. Usually for most models it is very difficult to take the effect of micro crack, rumpling interface and possible relatively large cracks into consideration. These features may have significant effect on the residual strain distribution inside the coating.

This method also can be applied to measure the strain distribution in any other direction. By integrating sectors of the Debye–Scherrer rings in the direction desired the XRD pattern diffracted from the crystallites lying preferentially can be reconstructed and refined giving a corresponding strain measurement.

It can be seen that this method of measuring residual stress distribution by synchrotron radiation in transmission geometry by area detector can precisely reveal the strain trend inside the TBC top coat as a function of depth. This method is not limited to this kind of material, it can also be used to measure the residual stress distribution in ceramic/metal layered structure such as brazing joint and ceramic coatings.

References

[1] C.H. Hsueh, E.R. Fuller, Scr. Mater. 42 (8) (2000) 781–787.
[2] E. Atar, C. Sarioglu, U. Demirler, et al., Scr. Mater. 48 (9) (2003) 1331–1336.
[3] J. Cao, C. Li, X. Song, J. Feng, X. Lin, Int. J. Appl. Ceram. Technol. (2013), http://dx.doi.org/10.1111/ijac.12185.
[4] J. Cao, H.Q. Wang, J.L. Qi, et al., Scr. Mater. 65 (3) (2011) 261–264.
[5] C. Zhou, N. Wang, Z. Wang, et al., Scr. Mater. 51 (10) (2004) 945–948.
[6] A.G. Evans, D.R. Mumm, J.W. Hutchinson, et al., Prog. Mater. Sci. 46 (5) (2001) 505–553.
[7] N.P. Padture, M. Gell, E.H. Jordan, Science 296 (5566) (2002) 280–284.
[8] X. Zhao, P. Xiao, Mater. Sci. Forum 606 (2009) 1–26.
[9] D. Liu, M. Seraffon, P.E.J. Flewitt, et al., J. Eur. Ceram. Soc. 33 (15) (2013) 3345–3357.
[10] M. Tanaka, M. Hasegawa, A.F. Dericioglu, et al., Mater. Sci. Eng. A 419 (1) (2006) 262–268.
[11] A.M. Limarga, R. Vaßen, D.R. Clarke, J. Appl. Mech. 78 (1) (2011) 011003.
[12] A.M. Limarga, J. Iveland, M. Gentleman, et al., Acta Mater. 59 (3) (2011) 1162–1167.
[13] T. Tomimatsu, S.J. Zhu, Y. Kagawa, Scr. Mater. 50 (1) (2004) 137–141.
[14] Q. Chen, W.G. Mao, Y.C. Zhou, et al., Appl. Surf. Sci. 256 (23) (2010) 7311–7315.
[15] M. Croft, Z. Zhong, N. Jisrawi, et al., Int. J. Fatigue 27 (10) (2005) 1408–1419.
[16] M. Croft, I. Zakharchenko, Z. Zhong, et al., J. Appl. Phys. 92 (1) (2002) 578–586.
[17] M. Croft, N. Jisrawi, Z. Zhong, et al., J. Eng. Mater. Technol. 130 (2) (2008) 021005.
[18] K. Knipe, A. Manero II, S.F. Siddiqui, et al., Nat. Commun. 5 (2014).
[19] S.J. Eichhorn, D.J. Scurr, P.M. Mummery, et al., J. Mater. Chem. 15 (10) (2005) 1106-1106.
[20] J. Thornton, D. Cookson, E. Pescott, Surf. Coat. Technol. 120 (1999) 96–102.
[21] J. Thornton, S. Slater, J. Almer, J. Am. Ceram. Soc. 88 (10) (2005) 2817–2825.
[22] P. Thompson, D.E. Cox, J.B. Hastings, J. Appl. Crystallogr. 20 (2) (1987) 79–83.
[23] B. Bondars, G. Heidemane, J. Grabis, et al., J. Mater. Sci. 30 (6) (1995) 1621–1625.
[24] TOPAS 4–2 Technical Reference Page 21.
[25] G. Lim, W. Parrish, C. Ortiz, et al., J. Mater. Res. 2 (04) (1987) 471–477.
[26] L. Yang, F. Yang, Y. Long, et al., Surf. Coat. Technol. 251 (2014) 98–105.
[27] J.A. Thompson, T.W. Clyne, Acta Mater. 49 (9) (2001) 1565–1575.
[28] D. Liu, O. Lord, O. Stevens, et al., Acta Mater. 61 (1) (2013) 12–21.
[29] X. Zhao, P. Xiao, Surf. Coat. Technol. 201 (3) (2006) 1124–1131.